European Journal of Medicinal Chemistry 73 (2014) 167–176

Contents lists available at ScienceDirect

European Journal of Medicinal Chemistry

journal homepage: http://www.elsevier.com/locate/ejmech

Original article

Structure-based design, synthesis and biological evaluation of diphenylmethylamine derivatives as novel Akt1 inhibitors

Tao Liu [a], Wenhu Zhan [a], Yanming Wang [a], Liangren Zhang [b], Bo Yang [c], Xiaowu Dong [a,*], Yongzhou Hu [a,**]

[a] ZJU-ENS Joint Laboratory of Medicinal Chemistry, Zhejiang Province Key Laboratory of Anti-Cancer Drug Research, College of Pharmaceutical Sciences, Zhejiang University, Hangzhou 310058, China
[b] State Key Laboratory of Natural and Biomimetic Drugs, Peking University, Beijing 100083, China
[c] Department of Pharmacology, Zhejiang University, Hangzhou 310058, China

ARTICLE INFO

Article history:
Received 29 August 2013
Received in revised form
15 November 2013
Accepted 24 November 2013
Available online 19 December 2013

Keywords:
Akt1 inhibitor
Diphenylmethylamine
Pharmacophore
Molecular docking
Anti-proliferative activity

ABSTRACT

A series of diphenylmethylamine derivatives were rationally designed, synthesized and biologically evaluated. Most of them exhibited moderate to good Akt1 inhibitory activities, as well as promising anti-proliferative efficacy against cancer cell lines. Besides, molecular docking studies were carried out to probe their binding modes with Akt1. Further kinase selectivity studies of compound **22c** were performed, indicating its excellent selectivity against Aurora A, Drak, IKKβ, GSK3β, SYK and JAK2, and moderate selectivity against PKC and BRAF. Finally, a refined pharmacophore model was generated using the most active compounds **2**, **12c** and **22c** via application of HipHop program.

1. Introduction

PKB/Akt, a serine/threonine kinase, functions as a key signaling node in the PI3K/Akt/mTOR pathway that plays a critical role in cell growth, proliferation, motility and survival [1–6]. Frequent activation of Akt kinases was observed in a wide assortment of human solid tumors and hematological malignancies [7,8]. Akt consists of three isoforms, known as Akt1, Akt2 and Akt3. Although these three isoforms are encoded by separate genes, the identity of their overall sequence is very high (~80%) [9,10]. Up to now, accumulating researches have validated that the inhibition of Akt1, Akt2 and Akt3 activities is closely linked to the decrease of tumor growth, the apoptosis of cancer cells, as well as the reverse of tumor resistance [11,12]. Neverthlessly, a strong interest has been stimulated in targeting Akt for cancer therapy, leading to the discovery of a number of Akt inhibitors [13–15]. Currently, several Akt inhibitors are being evaluated in clinical trials (Fig. 1), including phosphatidylinositol (3,4,5)-trisphosphate mimics (e.g. Perifosine) [16,17], allosteric inhibitors (e.g. MK-2206) [18] and ATP-competitive inhibitors (e.g. AZD5363 [19] and AT13148 [20]). However, there are still some issues that need to be resolved, such as selectivity and safety. Despite these, there continues to be a great interest in the development of novel Akt inhibitors. Owing to the availability of high resolution structures of Akt [16,19–21], structure-based drug design is a promising method to accelerate the discovery process of drug candidates.

In our previous studies, a virtual evaluation system, which consists of pharmacophore and molecular docking models, has been developed and demonstrated as a good tool in identification of Akt1 inhibitors [21]. As a continuous study (Fig. 2), the analogs of **1** [22] were generated "in silico" and submitted to virtual evaluation. The preliminary results revealed that both of **2** and **3** still showed good scores in pharmacophore and molecular docking models, when bulky alkyl group was introduce onto primary amine of **1** (e.g. isopropyl for **2** and cyclopropyl for **3**). Thus, there would be a novel optimization site for compound **1**, which is much different from that of others' work [22–24]. Moreover, the hypothesis was validated by the good Akt1 inhibitory activities of compounds **2** and **3** (IC_{50}, **2**: 0.16 μM; **3**: 0.47 μM), after these two compounds were synthesized and biologically evaluated. Accordingly, more extensively modification of diphenylmethylamine derivatives was performed, in attempt to improve their potency and/

* Corresponding author. Tel./fax: +86 571 88981051.
** Corresponding author. Tel./fax: +86 571 88208460.
E-mail addresses: dongxw@zju.edu.cn (X. Dong), huyz@zju.edu.cn (Y. Hu).

0223-5234/$ – see front matter © 2013 Elsevier Masson SAS. All rights reserved.
http://dx.doi.org/10.1016/j.ejmech.2013.11.036

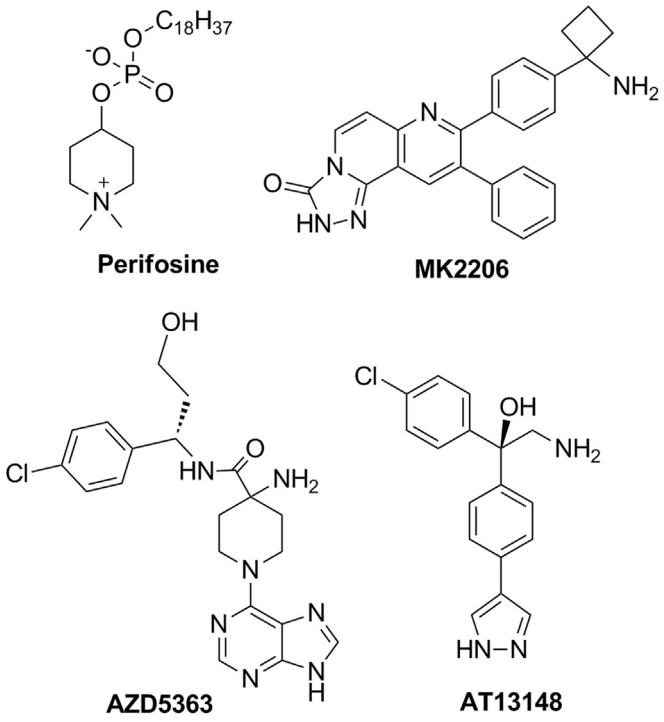

Fig. 1. The structure of representative Akt inhibitors under clinical trials.

or selectivity. Different substituents, including hydrophobic, hydrophilic, aliphatic and aromatic groups were introduced to primary amine of diphenylmethylamine skeleton, while replacing the purine moiety of the parent compound with pyridine and pyrazole, which are privileged fragments of numerous kinase inhibitors. Afterward, all of the designed compounds were synthesized and biologically evaluated. Insight into the structure–activities relationship (SAR), molecular docking studies were further performed and discussed. Moreover, a refined pharmacophore model was obtained by using newly synthesized compounds.

2. Computational methods

2.1. General methodology

Docking studies were achieved using Discovery Studio 2.5/Ligandfit module (Accelrys Inc., San Diego, CA). Pharmacophore mapping was performed using Discovery Studio 2.5/Pharmacophore module (Accelrys Inc., San Diego, CA). Diverse conformational models for each compound were generated by Discovery Studio 2.5/Pharmacophore module (Accelrys Inc., San Diego, CA) using an energy range of 20 kcal/mol of the calculated potential energy minimum. Specify 250 as the maximum number of conformers for each molecule to ensure maximum coverage of the conformational space. The refined pharmacophore model (HipHop) was also generated using the Discovery Studio 2.5/Pharmacophore module (Accelrys Inc., San Diego, CA).

2.2. Molecular docking with LigandFit

The docking site of Akt1 enzyme (PDB entry code: 3OCB) was derived using the LigandFit site search utility in Discovery studio 2.5 [25]. For the generation of the ligand's conformations, we used variable numbers of Monte Carlo simulations. All the calculations during the docking steps were performed under the PLP Force Field formalism. A short rigid body minimization was then performed and 50 poses for each ligand were saved. Scoring was performed with a set of scoring functions (including Dock_score, LigScore2, PLP1, Jain and PMF) implemented in LigandFit module. The

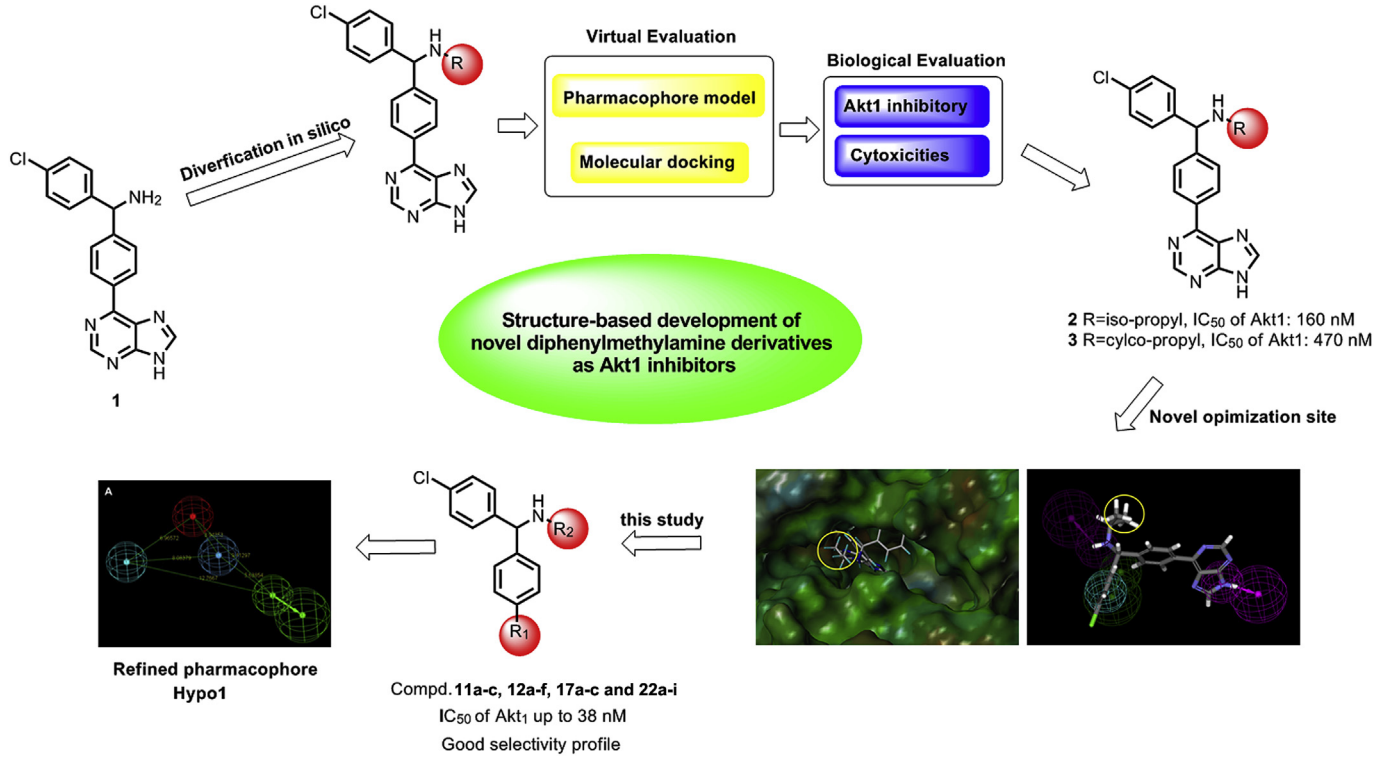

Fig. 2. The evolution of novel diphenylmethylamine derivatives as Akt inhibitors.

combination of consensus scoring method and the interaction mode was applied to select the preferable output conformation.

2.3. Generation of pharmacophore hypotheses with HipHop

Discovery Studio 2.5/HipHop module [26] was employed to evaluate the common features required for highly potency of Akt1 inhibitors. A training set consisting of compounds **2**, **12c** and **22c** was submitted for pharmacophore model generation based on common chemical features. All the parameters were kept at the default setting except the "best method" for the conformation generation and fitting.

3. Results and discussion

3.1. Chemistry

The synthetic route for compounds **2**, **3**, **11a**–**c**, **12a**–**g**, **17a**–**c** and **22a**–**j** is outlined in Scheme 1. Treatment of **4** with 4-bromophenyl magnesium bromide in Et_2O yielded diphenylmethanol **5**, which was successively transformed to the corresponding borate **6** by reaction with bis(pinacolato)diboron in presence of $Pd(PPh_3)_2Cl_2$ and KOAc in dioxane. Reaction of pyridine **7** with *n*-BuLi and triisopropyl borate in THF, followed by hydrolysis, yielded boronic acid **8** [27]. Compound **9** was obtained by Suzuki coupling of **8** with **5** in the presence of $Pd(PPh_3)_4$ and $NaHCO_3$ in DMF and water under microwave irradiation [28]. Afterward the 6-chloropurine **13** and 4-iodopyrazole **18** were protected by 3,4-dihydro-2*H*-pyran in presence of *p*-toluenesulfonic acid in CH_2Cl_2 to give **14** and **19**, respectively. Compounds **15** and **20** were obtained by Suzuki coupling of **14** and **19** with **6** and **5**, respectively. Then, chlorination of **9**, **15** and **20** with thionyl chloride in CH_2Cl_2 gave compounds **10**, **16** and **21**, respectively. Alkalization of **10**, **16** and **21** with appropriate amine under microwave irradiation yielded target compounds **2**, **3**, **11**, **12**, **17** and **22**.

3.2. Pharmacological activities

The Akt1 inhibitory activities of compounds **11a**–**c**, **12a**–**g**, **17a**–**c** and **22a**–**j** were determined via a competitive fluorescence polarization kinase activity assay. **H-89** [29] and staurosporine [30] were employed as positive control. Table 1 presents the biological results of tested compounds. With an insight into the modification of purine moiety of compound **1**, except for **12e** and **22f**, compounds **12**, **17**, and **22** bearing 4-pyridine, purine and pyrazole moieties showed much more potent Akt1 inhibitory activities than that of compound **11** bearing 3-pyridine moieties. It is suggested that the hydrogen bond interactions of heterocyclic moiety with Akt1 are essential. Comparing with the substituent on amino group of **2** and **22c**, the more bulky substituent (e.g. *N*-cyclohexyl for **17b** and *N*-benzyl for **17c**) and the longer substituent (e.g. *N*-isobutyl for **17a**, *N*-(2-hydroxy)ethyl for **22h** and *N*-(2-amino)ethyl for **22i**)

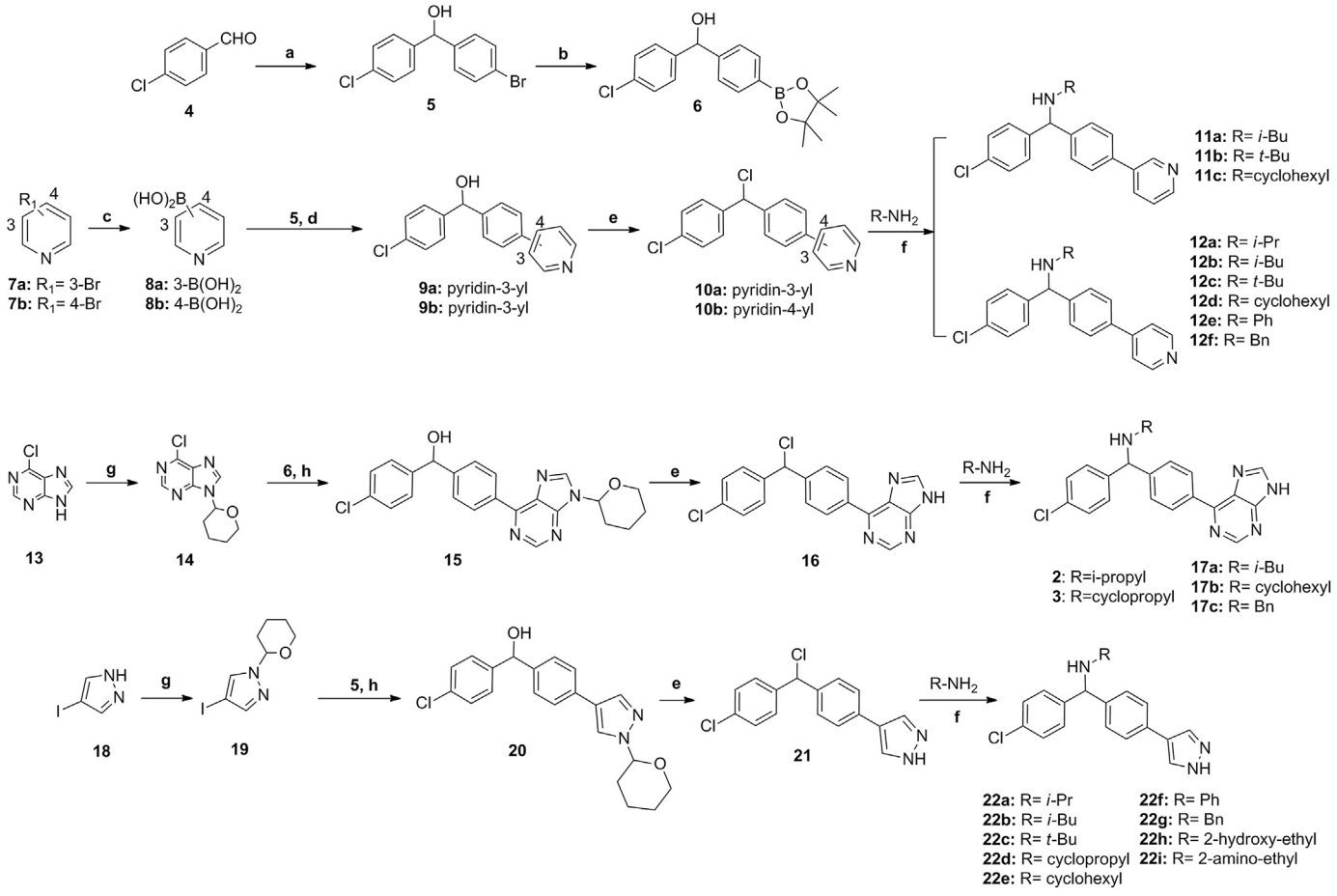

Scheme 1. The synthetic route for target compounds **2**, **3**, **11a**–**c**, **12a**–**g**, **17a**–**c** and **22a**–**j**. Reagents and conditions: (a) 4-bromophenyl magnesium bromide, Et_2O; (b) $Pd(PPh_3)_2Cl_2$, bis(pinacolato)diboron, KOAc, dioxane; (c) *n*-BuLi, triisopropyl borate, THF; (d) $Pd(PPh_3)_4$, $NaHCO_3$, DMF/H_2O, microwave; (e) $SOCl_2$, CH_2Cl_2; (f) appropriate amine, K_2CO_3, KI, CH_3CN, microwave; (g) 3,4-dihydro-2*H*-pyran, $TsOH \cdot H_2O$, CH_2Cl_2; (h) $Pd(PPh_3)_4$, Na_2CO_3, dioxane/H_2O, microwave.

Table 1
The Akt1 inhibitory and *in vitro* anti-proliferative activities of compounds **2**, **3**, **11a**–**c**, **12a**–**g**, **17a**–**c** and **22a**–**j**, against OVCAR-8, HL60 and HCT-116 cells.

Compd.	Akt1 inhibitory activity IC_{50}, μM (inhibition, %)[a]	Anti-proliferative activity (IC_{50}, μM)		
		OVCAR-8	HL60	HCT-116
Staurosporine	0.04	/	/	/
H-89	1.72	10.5	11.4	15.7
2	0.16	17.0	13.2	8.5
3	0.47	30.6	11.9	13.4
11a	(10%)[a]	N.T.[b]	N.T.[b]	N.T.[b]
11b	(19%)[a]	N.T.[b]	N.T.[b]	N.T.[b]
11c	(20%)[a]	N.T.[b]	N.T.[b]	N.T.[b]
12a	0.22	22.8	13.9	17.3
12b	1.43	16.3	3.3	15.5
12c	0.17	16.1	3.9	14.4
12d	1.26	15.6	3.2	12.4
12e	(26%)[a]	N.T.[b]	N.T.[b]	N.T.[b]
12f	1.25	18.5	12.5	16.3
17a	0.74	9.9	5.3	7.7
17b	0.64	8.6	11	14.4
17c	0.74	12.5	12.1	16.2
22a	0.37	12.2	10.7	11.6
22b	0.90	8.1	5.4	14.1
22c	0.038	8.1	5.3	8.9
22d	0.48	7.9	7.8	15.6
22e	1.1	5.5	2.1	26.8
22f	(29%)[a]	N. T.[b]	N.T.[b]	N.T.[b]
22g	1.32	11.9	5.3	8.3
22h	0.65	34.68	N.T.[b]	27.59
22i	0.82	11.05	N.T.[b]	10.73

[a] The inhibition rate of Akt1 activities was determined at a concentration of 10 μM.
[b] N.T. means no test.

decreased the Akt1 inhibitory activities. In addition, compounds **12e** and **22f** bearing *N*-phenyl group even showed no Akt1 inhibitory activity (inhibition rate of **12e** and **22f** were 26% and 29%, respectively, at a concentration of 10 μM), suggesting that aryl substituent on amino group of diphenylmethylamine skeleton is unfavorable. Overall, the *N*-*tert*-butyl group on diphenylmethylamine is the best substituent in both of pyridine and pyrazole series for Akt1 inhibitory activity (IC_{50}, **12c** IC_{50}; 0.17 μM, **22c** IC_{50}: 0.038 μM).

Furthermore, compounds **12a**–**d**, **12f**, **17a**–**c**, **22a**–**e** and **22g**–**i** with good Akt1 inhibitory activities were tested for their *in vitro* anti-proliferative activities against three human cancer cell lines including OVCAR-8 (Ovarian Adenocarcinoma), HL-60 (Promyelocytic Leukemia) and HCT116 (Human Colon Cancer). The results of them together with compounds **2** and **3** are summarized in Table 2. As expected, all of them exhibited moderate to potent anti-proliferative activities, especially for HL60 cell lines. Compound **22c**, the most potent one, also showed promising anti-proliferative activities against OVCAR-8 (IC_{50} = 8.1 μM), HL60 (IC_{50} = 5.3 μM), HCT-116 (IC_{50} = 8.9 μM) cells, which are better than that of compound **2** against OVCAR-8 (IC_{50} = 17.0 μM), HL60 (IC_{50} = 13.2 μM), HCT-116 (IC_{50} = 8.5 μM) cells. The preliminary mechanisms on the anti-proliferative activities against Ovcar-8 cells of **22c** were studied. At first, the effect of **22c** on the apoptosis of OVCAR-8 cells assessed using propidium iodide (PI) staining of the sub-G1 cell population. As shown in Fig. 3A, exposure of OVCAR-8 cells to **22c** for 48 h led to the apoptosis of 66.8% cells, while the negative control only induced the apoptosis of 1.2% cells. Then, the effect of **22c** on Akt phosphorylation was tested on OVCAR-8 cells. Treatment of OVCAR-8 cells with **22c** resulted in down-regulation of phosphorylated Akt (Ser-473), as well as phosphorylated GSK3β which is one of the major downstream targets of Akt, while no significant changes in overall total GSK3β and GAPDH protein levels were observed (Fig. 3B).

3.3. Kinase selectivity assay

The selectivity profile of **22c** is summarized in Table 2. The non-selective kinase inhibitor staurosporine was used as a control. Overall, compound **22c** demonstrates excellent selectivity against distinct families of kinases including Aurora A, Drak, IKKβ, GSK3β, SYK and JAK2, for which the IC_{50} values were greater than 2.5 μM. However, selectivity versus other closely related kinases such as BRAF1 (22-fold) and PKC (85-fold) are moderate, which may be attributed to the high degree of homology in the ATP-binding pocket.

3.4. Molecular docking studies using LigandFit

With the aim to further probe the SAR of tested compounds, the interaction mode between Akt1 and the good Akt1 inhibitors **12a**, **12c**, **17a**–**c**, **22a**–**d** and **22g**–**h**, the IC_{50} value of which were lower than 1 μM, were proposed and simulated by Discovery studio 2.5/LigandFit module. All of the scoring functions (DOCK_Score [25], LigScore2 [31], −PLP1 [32] and −PMF [33]) available in LigandFit program were applied for the evaluation of accuracy and reliability of molecular docking. Besides, the key interactions formed between Akt1 and the docked ligands were also emphasized as essential scoring parameters. Table 3 presents the molecular docking results of synthesized compounds. Most of the simulated compounds showed good consensus results, with good performance in more than three scoring functions. As exemplified by **22c**, the scores from DOCK_Score, LigScore2, PLP1 and PMF of **22c** (DOCK_Score: 83.6; LigScore2: 5.0; −PLP1: 88.0; −PMF: 70.7) are preferable. Further, the interactions with the key amino acid residues of Akt1 were highlighted and the distances were recorded. The interaction mode between Akt1 and **2**, **12c** and **22c** which exhibited the most potent inhibitory activities are presented in Fig. 4A–C. Two hydrogen bonds are formed between **22c** (or **2**) and Glu228 and Ala 230 of Akt1, respectively, while one hydrogen bond is formed between **12c** and Ala 230 of Akt1. All of the secondary amine of **2**, **12c** and **22c** can form ionic interaction with Glu234 of Akt1. In addition, the hydrophobic force between 4-chlorophenyl group of **2**, **12c** and **22c** and Phe161 of Akt1 serves to increase the thermal stability of the complex. Overall, the conformation and orientation of **2**, **12c** and **22c** are similar when their structure were mapping together (Fig. 4D).

3.5. Refined pharmacophore model established by HipHop program

With aim to improve the prediction ability of the pharmacophore model for diphenylmethylamine derivatives, three highly active compounds **2**, **12c** and **22c** with different heterocyclic

Table 2
Selectivity profile of **22c** in comparison with that of staurosporine.

Test kinases	Compd. **22c** IC_{50}, μM (inhibition, %)[a]	Staurosporine IC_{50}, μM
Akt1	0.038	0.040
Aurora A	(28.3%)[a]	0.015
BRAF1	0.88	0.015
PKC	3.4	0.001
Drak	(12.0%)[a]	0.026
IKKβ	(1.8%)[a]	0.001
GSK3β	(7.2%)[a]	0.072
SYK	(0.98%)[a]	0.060
JAK2	(19.5%)[a]	0.002

[a] The inhibition rate was determined at a concentration of 0.8 μg/mL.

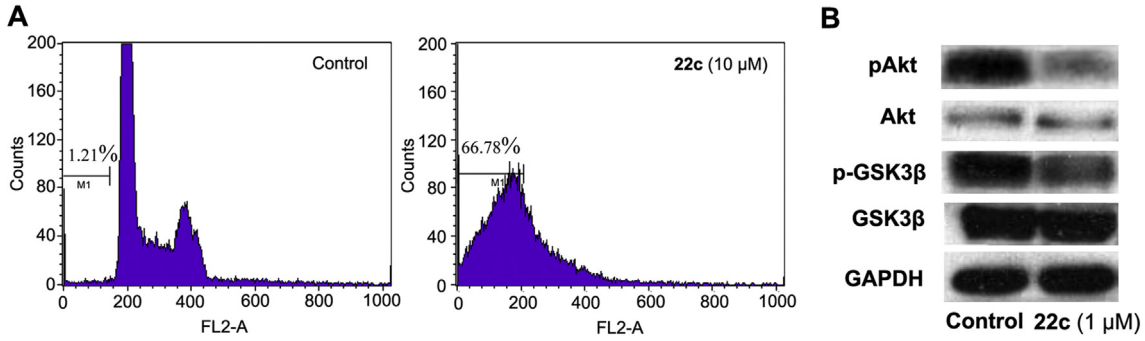

Fig. 3. (A) cell apoptotic index analyses of OVCAR-8 cells exposed to **22c**; (B) treatment with **22c**-caused decrease of Akt and GSK3β phosphorylation in OVCAR-8 cells.

moieties attached to diphenylmethylamine skeleton were chosen as a training set to generate the refined pharmacophore model. Ten pharmacophore models were obtained and the best pharmacophore model (Hypo1) with the highest score 32.76 contained four chemical features: one pos-ionizable (PI), two hydrophobic (HP), and one hydrogen bond acceptor (HBA) (Fig. 5A). Compound **22c**, the most potent one, mapped well with all of the four features of Hypo1 (Fig. 5B). It is suggested that the refined pharmacophore would be good tool not only in further structural optimization of diphenylmethylamine derivatives as potent and selective Akt1 inhibitors, but also in the identification of novel Akt1 inhibitors.

4. Conclusion

The rational strategy combined with virtual evaluation and experimental feedback were performed for the structural optimization of diphenylmethylamine derivative as potent Akt1 inhibitors. Particularly, the modification on the novel site of diphenylmethylamines was extensively carried out. The biological assay reveals that most of the synthesized compounds possessed both of good Akt1 inhibitory activities and anti-proliferative activities against cancer cells. Favorable selectivity profile of representative compound **22c** was also observed. Therefore, the most promising compounds **2**, **12c** and **22c** would be interesting leads for further structure–activity relationship exploration and structurally optimization. Furthermore, the HipHop pharmacophore model was constructed based on the common features of highly active compounds **2**, **12c** and **22c**. The application of this refined pharmacophore model is undergoing for the development of Akt1 inhibitors with novel skeleton.

Table 3
The molecular docking results of **2**, **3**, **12a**, **12c**, **17a–c**, **22a–d** and **22g–h**.

Compd.	DOCK_ Score	LigScore2	−PLP1	−PMF	Key interaction (distance, Å)		
					Ala232	Glu230	Glu234
2	96.3	2.9	103.8	100.0	2.08	2.08	4.42
3	96.8	4.0	103.7	78.0	2.10	2.06	4.44
12a	92.5	3.5	97.5	77.8	2.08	/	4.03
12c	89.0	4.4	93.3	72.3	1.97	/	3.45
17a	97.6	3.3	104.1	83.0	1.92	1.82	4.14
17b	99.1	4.28	100.9	78.9	2.07	2.03	4.40
17c	104.8	3.1	108.8	70.1	2.59	2.73	4.19
22a	84.3	4.7	87.7	63.6	2.00	2.23	3.02
22b	83.4	4.91	91.2	61.3	2.21	2.59	3.26
22c	83.6	5.0	87.1	66.1	1.91	2.25	2.81
22d	86.0	4.6	90.8	74.5	1.88	2.25	2.64
22h	87.7	5.1	92.6	69.5	2.09	2.48	3.03
22i	89.7	5.0	92.3	66.7	2.05	2.37	4.32

5. Experimental

5.1. Chemistry

Melting points were obtained on a B-540 Büchi melting-point apparatus and are uncorrected. ^{1}H NMR spectra were recorded on a 500 MHz ^{1}H and 400 MHz. ^{13}C NMR were recorded on a 125 MHz and 100 MHz spectrometer, respectively (chemical shifts are given in ppm (δ) relative to TMS as internal standard, coupling constants (J) are in hertz (Hz), and signals are designated as follows: s, singlet; d, doublet; t, triplet; m, multiplet; br s, broad singlet, etc.). Mass spectral data were obtained on an Esquire-LC-00075 spectrometer. High resolution mass spectra were measured on an Agilent 1290 HPLC-6224 Time of Fight Mass Spectrometer.

5.1.1. (4-Bromophenyl)(4-chlorophenyl)methanol **5**

To a cooled solution of 4-bromobenzaldehyde (10.4 g, 56 mmol) in dry THF (30 ml) was added dropwise 4-chlorophenylmagnesium bromide (60 ml, 1 N solution in THF, 60 mmol). The solution was stirred for 2 h, and then saturated ammonium chloride (300 ml) was added, followed by ethyl acetate (250 ml). The layers were separated, and the organic fraction was washed with water (100 ml), then dried, concentrated and purified by flash column chromatography to afford the desired product (yield, 62%) as a white solid, mp 100–102 °C; ^{1}H NMR (500 MHz, $CDCl_3$) δ 7.47 (d, J = 8.3 Hz, 2H), 7.31 (q, J = 8.4 Hz, 4H), 7.24 (d, J = 8.2 Hz, 2H), 5.78 (s, 1H). ESI-MS (m/z): 297 $[M + 1]^+$.

5.1.2. (4-Chlorophenyl)(4-(4,4,5,5-tetramethyl-1,3,2-dioxaborolan-2-yl)phenyl)methanol **6**

To a solution of compound **5** (297 mg, 1 mmol) in dioxane (5 ml) was added bis(pinacolato)diboron (280 mg, 1.1 mmol), $Pd(PPh_3)_2Cl_2$(23.65 mg, 0.0337 mmol), and KOAc (252 mg, 3 mmol). The reaction mixture was heated to 85 °C in a sealed tube for 12 h. The reaction solution was poured into H_2O (20 ml) and extracted with ethyl acetate (15 ml × 3). The combined organic layers were dried over anhydrous Na_2SO_4, concentrated under vacuum and purified on silica gel to afford the title compound as a white solid (yield, 61%), mp 116–118 °C. ^{1}H NMR (500 MHz, DMSO) δ 7.64–7.59 (m, 2H), 7.41–7.33 (m, 6H), 5.72 (d, J = 3.8 Hz, 1H), 1.27 (s, 12H). ESI-MS (m/z): 345 $[M + 1]^+$.

5.1.3. General procedure for the synthesis of compound **8**

To a solution of compound **5** (100 mg, 0.33 mmol) in 4 ml dioxane/H_2O (3:2, v/v) was added compound **7** (62 mg, 0.5 mmol), tetrakistriphenylphosphane Pd (0) (5 mol%), and $NaHCO_3$ (126 mg, 1.5 mmol). The reaction mixture was heated to 100 °C in a sealed tube for 6 h. The reaction solution was poured into H_2O (25 ml) and

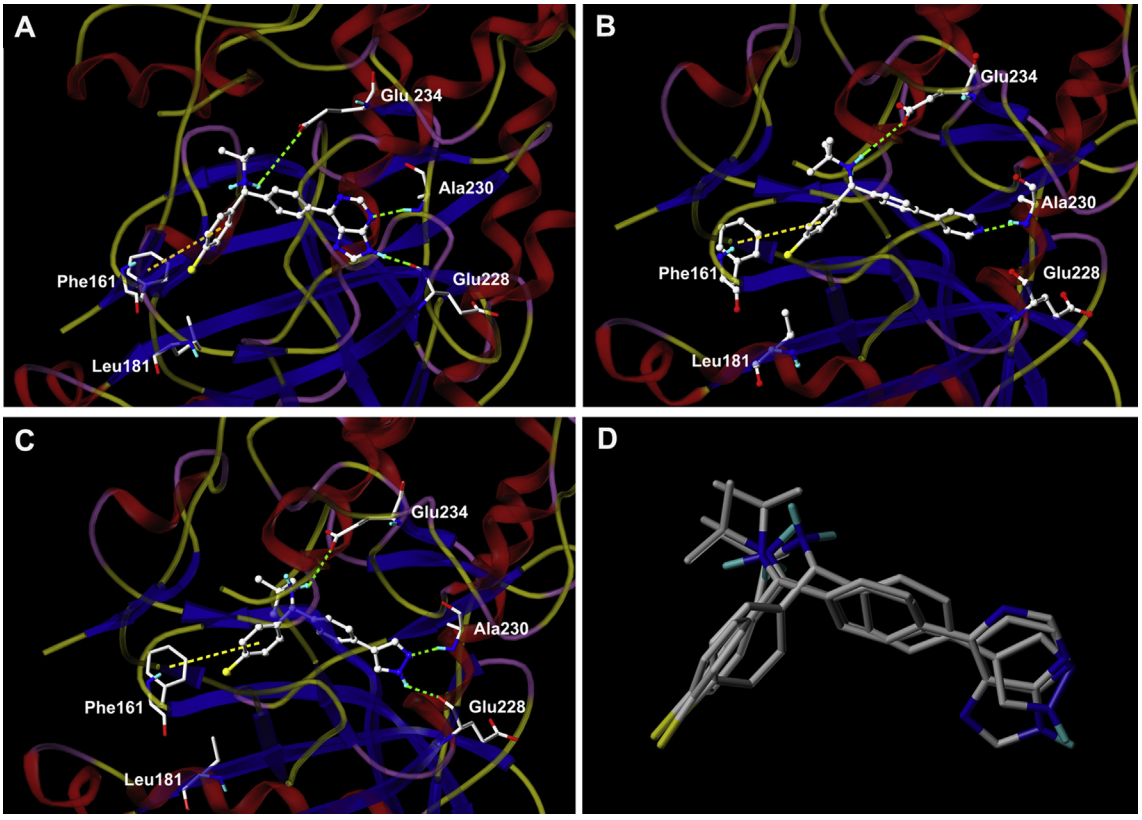

Fig. 4. Interaction mode between Akt1 and **22c** (A), **2** (B), **12c** (C) with Akt1, hydrogen bond interaction was highlighted using yellow dash line, hydrophobic force was highlighted using yellow dash line; (D) the aliment of **2**, **12c** and **22c**. (For interpretation of the references to color in this figure legend, the reader is referred to the web version of this article.)

extracted with ethyl acetate (15 ml × 3). The combined organic layers were dried over Na_2SO_4, concentrated under vacuum and purified on silica gel to afford title compounds.

*5.1.3.1. Pyridin-3-ylboronic acid **8a**.* Pale yellow solid (yield, 91%), mp: 152–155 °C. ^{1}H NMR (500 MHz, DMSO) δ 8.89 (d, J = 1.9 Hz, 1H), 8.58 (dd, J = 4.8, 1.3 Hz, 1H), 8.16–8.05 (m, 1H), 7.69 (d, J = 8.3 Hz, 2H), 7.54–7.48 (m, 3H), 7.44 (d, J = 8.5 Hz, 2H), 7.41–7.36 (m, 2H), 5.76 (s, 1H). ESI-MS (m/z): 296 $[M + 1]^+$.

*5.1.3.2. Pyridin-4-ylboronic acid **8b**.* Yellow solid (yield, 78%), mp: 153–155 °C. ^{1}H NMR (500 MHz, $CDCl_3$) δ 8.62 (s, 2H), 7.55 (dd, J = 6.5, 1.7 Hz, 2H), 7.51–7.44 (m, 4H), 7.41–7.34 (m, 2H), 7.24 (d, J = 8.4 Hz, 2H), 5.03 (s, 1H). ESI-MS (m/z): 296 $[M + 1]^+$.

*5.1.4. General procedure for the synthesis of compounds **14** and **19***

A suspension of 6-chloro-9*H*-purine (or 4-iodo-1*H*-pyrazole) (13 mmol) and 4-methylbenzenesulfonic acid (0.12 g, 0.65 mmol) in EtOAc (25 ml) was treated with 3,4-dihydro-2*H*-pyran (3.54 ml,

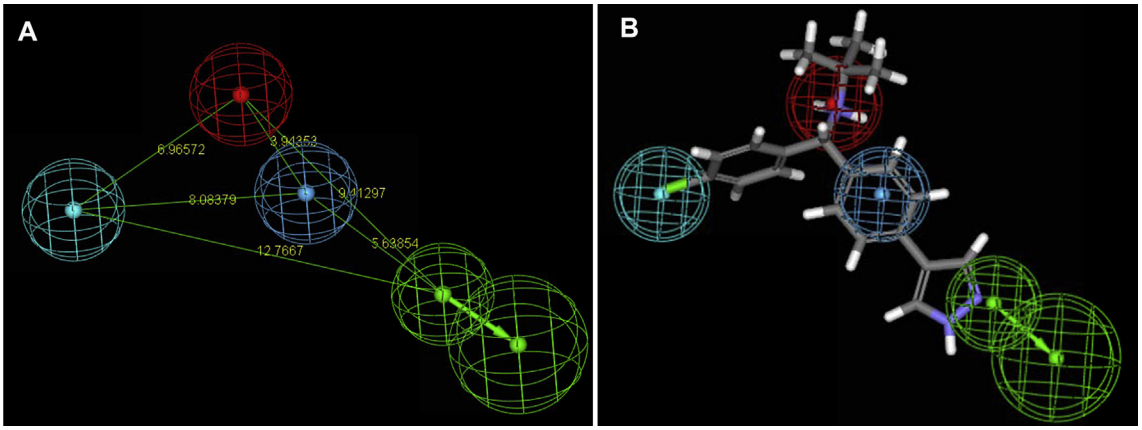

Fig. 5. Hypo1 and its mapping to representative compounds. (A) The topological features of Hypo1: the cyan contour represents hydrophobic (HY), green contour represents hydrogen bond acceptor (HBA), and red contour represents pos-ionizable (PI) features; (B) compound **22c** mapped with Hypo1. (For interpretation of the references to color in this figure legend, the reader is referred to the web version of this article.)

39 mmol). The mixture was heated at 90 °C and the solid slowly dissolved over 1 h. The flask was removed from the oil bath and the cloudy yellow solution was filtered and concentrated under vacuum. The pale yellow residue was purified by flash chromatography to give title compound.

5.1.4.1. 6-Chloro-9-(tetrahydro-2H-pyran-2-yl)-9H-purine ***14***. White solid (yield, 89%), mp 70–71 °C. ^{1}H NMR (500 MHz, $CDCl_3$) δ 8.76 (s, 1H), 8.35 (s, 1H), 5.80 (dd, J = 10.5, 2.4 Hz, 1H), 4.24–4.15 (m, 1H), 3.80 (td, J = 11.7, 2.7 Hz, 1H), 2.22–2.15 (m, 1H), 2.14–2.01 (m, 2H), 1.86–1.73 (m, 2H), 1.71–1.64 (m, 1H). ESI-MS (m/z): 239 $[M + 1]^+$.

5.1.4.2. 4-Iodo-1-(tetrahydro-2H-pyran-2-yl)-1H-pyrazole ***19***. Yellow oil (yield, 80%). ^{1}H NMR (500 MHz, $CDCl_3$) δ 7.67 (s, 1H), 7.55 (s, 1H), 5.38 (dd, J = 8.2, 3.7 Hz, 1H), 4.08–3.99 (m, 1H), 3.73–3.63 (m, 1H), 2.14–1.96 (m, 3H), 1.75–1.58 (m, 3H). ESI-MS (m/z): 279 $[M + 1]^+$.

5.1.5. General procedure for the synthesis of compounds ***15*** *and* ***20***

To a solution of compound **14** (or **19**) (0.44 mmol) in 15 ml DMF/H_2O (3:2, v/v) was added compound **11** (207 mg, 0.44 mmol), tetrakistriphenylphosphane palladium (5 mol %), and Na_2CO_3 (138 mg, 1.3 mmol). The reaction mixture was heated to 110 °C in a sealed tube for 6 h. The reaction solution was poured into H_2O (50 ml) and extracted with ethyl acetate (25 ml × 3). The combined organic layers were dried over Na_2SO_4, concentrated under vacuum and purified on silica gel to afford the title compound.

5.1.5.1. (4-Chlorophenyl)(4-(9-(tetrahydro-2H-pyran-2-yl)-9H-purin-6-yl)phenyl)methanol ***15***. White solid (yield, 67%), mp: 151–153 °C. ^{1}H NMR (500 MHz, $CDCl_3$) δ 7.84 (s, 1H), 7.80 (s, 1H), 7.48 (d, J = 8.0 Hz, 2H), 7.38 (d, J = 8.0 Hz, 2H), 7.32 (d, J = 8.0 Hz, 2H), 7.25 (d, J = 8.0 Hz, 2H), 5.82 (dd, J = 9.2, 3.0 Hz, 1H), 4.25–4.12 (m, 1H), 5.77 (s, 1H), 3.83–3.72 (m, 1H), 2.20–2.00 (m, 3H), 1.82–1.58 (m, 3H). ESI-MS (m/z): 421 $[M + 1]^+$.

5.1.5.2. (4-Chlorophenyl)(4-(1-(tetrahydro-2H-pyran-2-yl)-1H-pyrazol-4-yl)phenyl)methanol ***20***. Yellowish solid (yield, 76%), mp: 125–127 °C. ^{1}H NMR (500 MHz, $CDCl_3$) δ 7.84 (s, 1H), 7.80 (s, 1H), 7.46 (d, J = 8.0 Hz, 2H), 7.38 (d, J = 8.0 Hz, 2H), 7.32 (d, J = 8.0 Hz, 2H), 7.25 (d, J = 8.0 Hz, 2H), 5.82 (s, 1H), 5.41 (dd, J = 9.2, 3.0 Hz, 1H), 4.11–4.05 (m, 1H), 3.73–3.63 (m, 1H), 2.22–2.01 (m, 3H), 1.80–1.57 (m, 3H). ESI-MS (m/z): 369 $[M + 1]^+$.

5.1.6. General procedure for the synthesis of compounds ***10***, ***16*** *and* ***21***

To a solution of **9** (**15**, or **20**) (0.2 mmol) in anhydrous CH_2Cl_2 (4 ml) at 0 °C was added $SOCl_2$ (1.2 mmol) in one portion. The solution stirred at 25 °C for 6 h and was then poured into ice-water and extracted with ethyl acetate (20 ml × 3). The organic phase was washed with brine, dried over anhydrous Na_2SO_4, and then concentrated under vacuum to title compound without further purification. Then, it was immediately dissolved in CH_3CN (2 ml) was added the appropriate amine (2 mmol), K_2CO_3 (55 mg, 0.4 mmol) and KI (1.66 mg, 0.01 mmol). The reaction mixture was irradiated with microwaves for 20 min at 140 °C and was then poured into water (20 ml). The mixture was extracted with ethyl acetate (10 ml × 3). The combined organic layer was dried over anhydrous $NaSO_4$, concentrated and purified on silica gel to afford the title compound.

5.1.6.1. N-((4-Chlorophenyl) (4-(pyridin-3-yl)phenyl)methyl)-2-methylpropan-1-amine ***11a***. White solid (yield, 38%), mp: 86–88 °C. ^{1}H NMR (500 MHz, $CDCl_3$) δ 8.81 (d, J = 1.7 Hz, 1H), 8.57 (d, J = 4.8 Hz, 1H), 7.86–7.80 (m, 1H), 7.55–7.48 (m, 4H), 7.41 (d, J = 8.0 Hz, 2H), 7.35 (dd, J = 8.0, 4.8 Hz, 1H), 7.29 (d, J = 8.0 Hz, 2H), 4.85 (s, 1H), 2.48–2.38 (m, 2H), 1.81 (dq, J = 13.3, 6.6 Hz, 1H), 0.94 (d, J = 6.6 Hz, 6H). ESI-MS (m/z): 351 $[M + 1]^+$, HRMS (ESI): m/z calcd for $(C_{22}H_{23}ClN_2 + H)^+$: 351.1628; found: 351.1630.

5.1.6.2. N-((4-Chlorophenyl)(4-(pyridin-3-yl)phenyl)methyl)-2-methylpropan-2-amine ***11b***. Yellow solid (yield, 29%), mp: 100–102 °C. ^{1}H NMR (500 MHz, $CDCl_3$) δ 8.80 (s, 1H), 8.57 (s, 1H), 7.86–7.80 (m, 1H), 7.55–7.46 (m, 4H), 7.43 (d, J = 8.0 Hz, 2H), 7.34 (dd, J = 8.0, 4.8 Hz, 1H), 7.27 (d, J = 8.0 Hz, 2H), 5.08 (s, 1H), 1.11 (s, 9H). ESI-MS (m/z): 351 $[M + 1]^+$. HRMS (ESI): m/z calcd for $(C_{22}H_{23}ClN_2 + H)^+$: 351.1628; found: 351.1635.

5.1.6.3. N-((4-Chlorophenyl)(4-(pyridin-3-yl)phenyl)methyl)cyclohexanamine ***11c***. Yellow solid (yield, 39%), mp: 104–105 °C. ^{1}H NMR (500 MHz, $CDCl_3$) δ 8.81 (d, J = 1.9 Hz, 1H), 8.57 (d, J = 3.6 Hz, 1H), 7.88–7.80 (m, 1H), 7.52 (d, J = 8.0 Hz, 2H), 7.47 (d, J = 8.0 Hz, 2H), 7.37 (d, J = 8.0 Hz, 2H), 7.35–7.32 (m, 1H), 7.30–7.27 (m, 2H), 5.07 (s, 1H), 2.41 (dd, J = 11.6, 8.1 Hz, 1H), 1.97 (d, J = 10.1 Hz, 2H), 1.70 (d, J = 6.0 Hz, 2H), 1.22–1.03 (m, 6H). ESI-MS (m/z): 377 $[M + 1]^+$. HRMS (ESI): m/z calcd for $(C_{24}H_{25}ClN_2 + H)^+$: 377.1785; found: 377.1795.

5.1.6.4. N-((4-Chlorophenyl)(4-(pyridin-4-yl)phenyl)methyl)propan-2-amine ***12a***. Yellow solid (yield, 21%), mp: 75–77 °C. ^{1}H NMR (500 MHz, $CDCl_3$) δ 8.64 (d, J = 5.7 Hz, 2H), 7.58 (d, J = 8.0 Hz, 2H), 7.49 (d, J = 8.0 Hz, 2H), 7.47 (d, J = 5.8 Hz, 2H), 7.37 (d, J = 7.8 Hz, 2H), 7.28 (d, J = 8.0 Hz, 2H), 5.01 (s, 1H), 2.76 (dt, J = 12.6, 6.2 Hz, 1H), 1.10 (dd, J = 6.1, 1.0 Hz, 6H). ESI-MS (m/z): 337 $[M + 1]^+$. HRMS (ESI): m/z calcd for $(C_{21}H_{21}ClN_2 + H)^+$: 337.1472; found: 337.1467.

5.1.6.5. N-((4-Chlorophenyl)(4-(pyridin-4-yl)phenyl)methyl)-2-methylpropan-1-amine ***12b***. Yellow solid (yield, 39%), mp: 91–93 °C. ^{1}H NMR (500 MHz, $CDCl_3$) δ 8.65 (s, 2H), 7.60 (s, 4H), 7.47 (s, 4H), 7.31 (d, J = 7.7 Hz, 2H), 4.93 (s, 1H), 2.47 (s, 1H), 1.91–1.82 (m, 1H), 1.26 (s, 1H), 0.94 (d, J = 5.2 Hz, 4H). ^{13}C NMR (100 MHz, $CDCl_3$) δ 148.6, 148.4, 136.3, 134.4, 130.9, 130.7, 129.0, 128.9, 128.2, 127.6, 123.7, 66.6, 55.9, 27.8, 20.9. ESI-MS (m/z): 351 $[M + 1]^+$. HRMS (ESI): m/z calcd for $(C_{22}H_{23}ClN_2 + H)^+$: 351.1628; found: 351.1635.

5.1.6.6. N-((4-Chlorophenyl)(4-(pyridin-4-yl)phenyl)methyl)-2-methylpropan-2-amine ***12c***. Yellow solid (yield, 46%), mp: 85–87 °C. ^{1}H NMR (500 MHz, $CDCl_3$) δ 8.62 (s, 2H), 7.56 (dd, J = 6.5, 1.7 Hz, 2H), 7.51–7.44 (m, 4H), 7.41–7.34 (m, 2H), 7.26 (d, J = 8.4 Hz, 2H), 5.05 (s, 1H), 1.09 (s, 9H). ^{13}C NMR (100 MHz, $CDCl_3$) δ 150.4, 148.1, 136.7, 132.6, 131.6, 130.8, 128.9, 128.7, 128.2, 127.3, 121.6, 60.8, 52.2, 30.2. ESI-MS (m/z): 351 $[M + 1]^+$. HRMS (ESI): m/z calcd for $(C_{22}H_{23}ClN_2 + H)^+$: 351.1628; found: 351.1618.

5.1.6.7. N-((4-Chlorophenyl)(4-(pyridin-4-yl)phenyl)methyl)cyclohexanamine ***12d***. Orange solid (yield 36%), mp: 73–75 °C. ^{1}H NMR (500 MHz, $CDCl_3$) δ 8.64 (dd, J = 4.7, 1.4 Hz, 2H), 7.58 (d, J = 8.1 Hz, 2H), 7.48 (t, J = 7.8 Hz, 4H), 7.36 (d, J = 8.3 Hz, 2H), 7.28 (d, J = 8.4 Hz, 2H), 5.07 (s, 1H), 2.40 (t, J = 9.7 Hz, 1H), 1.96 (s, 2H), 1.70 (d, J = 5.6 Hz, 2H), 1.57 (s, 2H), 1.20–1.09 (m, 4H). ESI-MS (m/z): 377 $[M + 1]^+$. HRMS (ESI): m/z calcd for $(C_{24}H_{25}ClN_2 + H)^+$: 376.1706; found: 376.1710.

5.1.6.8. N-((4-Chlorophenyl)(4-(pyridin-4-yl)phenyl)methyl)aniline ***12e***. Orange solid (yield, 42%), mp: 114–116 °C. ^{1}H NMR (500 MHz, $CDCl_3$) δ 8.66 (s, 2H), 7.62 (d, J = 7.4 Hz, 2H), 7.53 (d, J = 4.0 Hz, 2H), 7.47 (d, J = 7.2 Hz, 2H), 7.33 (s, 4H), 7.15 (t, J = 7.2 Hz, 2H), 6.74 (t, J = 7.3 Hz, 1H), 6.56 (d, J = 7.7 Hz, 2H), 5.53 (s, 1H). ESI-MS (m/z):

371 [M + 1]$^+$. HRMS (ESI): *m/z* calcd for ($C_{24}H_{19}ClN_2$ + H)$^+$: 371.1315; found: 371.1318.

5.1.6.9. N-Benzyl-1-(4-chlorophenyl)-1-(4-(pyridin-4-yl)phenyl) methanamine ***12f***. Yellow solid (yield, 46%), mp: 77–79 °C. ^{1}H NMR (500 MHz, $CDCl_3$) δ 8.63 (dd, J = 4.7, 1.4 Hz, 2H), 7.59 (d, J = 8.2 Hz, 2H), 7.53 (d, J = 8.3 Hz, 2H), 7.47 (dd, J = 4.6, 1.6 Hz, 2H), 7.42–7.39 (m, 2H), 7.37–7.27 (m, 7H), 4.90 (s, 1H), 3.76 (s, 2H). ^{13}C NMR (100 MHz, $CDCl_3$) δ 150.2, 147.9, 147.2, 137.2, 133.2, 130.8, 129.5, 128.9, 128.6, 128.4, 128.1, 127.5, 127.4, 127.3, 121.5, 65.2, 51.5. ESI-MS (*m/z*): 385 [M + 1]$^+$. HRMS (ESI): *m/z* calcd for ($C_{25}H_{21}ClN_2$ + H)$^+$: 385.1472; found: 385.1486.

5.1.6.10. N-((4-(9H-Purin-6-yl)phenyl)(4-chlorophenyl)methyl) propan-2-amine ***2***. Yellow solid (yield, 20%), mp: 109–111 °C. ^{1}H NMR (500 MHz, $CDCl_3$) δ 8.93 (s, 1H), 8.64 (d, J = 7.9 Hz, 2H), 8.26 (s, 1H), 7.62 (d, J = 8.2 Hz, 2H), 7.44 (d, J = 8.3 Hz, 2H), 7.29 (d, J = 8.3 Hz, 2H), 5.16 (s, 1H), 3.02–2.89 (m, 1H), 1.21 (t, J = 6.8 Hz, 6H). ESI-MS (*m/z*): 378 [M + 1]$^+$. HRMS (ESI): *m/z* calcd for ($C_{21}H_{20}ClN_5$ + H)$^+$: 378.1485; found: 378.1480.

5.1.6.11. N-((4-(9H-Purin-6-yl)phenyl)(4-chlorophenyl)methyl)cyclopropanamine ***3***. White solid (yield, 47%), mp: 79–81 °C. ^{1}H NMR (500 MHz, $CDCl_3$) δ 8.98 (s, 1H), 8.74 (d, J = 8.4 Hz, 2H), 8.28 (s, 1H), 7.55 (d, J = 8.3 Hz, 2H), 7.32 (d, J = 8.5 Hz, 2H), 7.27 (d, J = 8.5 Hz, 2H), 4.99 (s, 1H), 2.11–2.08 (m, 1H), 0.48–0.36 (m, 4H). ESI-MS (*m/z*): 376 [M + 1]$^+$. HRMS (ESI): *m/z* calcd for ($C_{21}H_{18}ClN_5$ + H)$^+$: 376.1329; found: 376.1331.

5.1.6.12. N-((4-(9H-Purin-6-yl)phenyl)(4-chlorophenyl)methyl)-2-methylpropan-1-amine ***17a***. White solid (yield, 39%), mp: 87–90 °C. ^{1}H NMR (500 MHz, $CDCl_3$) δ 8.96 (s, 1H), 8.72 (d, J = 8.1 Hz, 2H), 8.27 (s, 1H), 7.60 (d, J = 8.3 Hz, 2H), 7.38 (d, J = 8.5 Hz, 2H), 7.27 (d, J = 8.3 Hz, 2H), 4.87 (s, 1H), 2.42 (d, J = 6.6 Hz, 2H), 1.86–1.74 (m, 1H), 0.93 (dt, J = 9.8, 4.9 Hz, 6H). ESI-MS (*m/z*): 392 [M + 1]$^+$. HRMS (ESI): *m/z* calcd for ($C_{22}H_{22}ClN_5$ + H)$^+$: 392.1642; found: 392.1652.

5.1.6.13. N-((4-(9H-Purin-6-yl)phenyl)(4-chlorophenyl)methyl)cyclohexanamine ***17b***. Yellow solid (yield, 32%), mp: 72–74 °C. ^{1}H NMR (500 MHz, $CDCl_3$) δ 9.02 (s, 1H), 8.71 (d, J = 8.1 Hz, 2H), 8.30 (s, 1H), 7.58 (d, J = 8.3 Hz, 2H), 7.37 (d, J = 8.4 Hz, 2H), 7.26 (d, J = 8.5 Hz, 2H), 5.12 (s, 1H), 2.44 (s, 1H), 2.03–1.91 (m, 2H), 1.69 (s, 2H), 1.20–1.07 (m, 6H). ESI-MS (*m/z*): 418 [M + 1]$^+$. HRMS (ESI): *m/z* calcd for ($C_{24}H_{24}ClN_5$ + H)$^+$: 418.1798; found: 418.1801.

5.1.6.14. 1-(4-(9H-Purin-6-yl)phenyl)-N-benzyl-1-(4-chlorophenyl) methanamine ***17c***. White solid (yield, 33%), mp: 118–120 °C. ^{1}H NMR (500 MHz, $CDCl_3$) δ 8.97 (s, 1H), 8.74 (d, J = 8.3 Hz, 2H), 8.28 (s, 1H), 7.62 (d, J = 8.3 Hz, 2H), 7.39 (t, J = 6.7 Hz, 2H), 7.36–7.32 (m, 4H), 7.28 (d, J = 8.4 Hz, 3H), 4.93 (s, 1H), 3.78 (d, J = 3.1 Hz, 2H). ESI-MS (*m/z*): 426 [M + 1]$^+$. HRMS (ESI): *m/z* calcd for ($C_{25}H_{20}ClN_5$ + H)$^+$: 426.1485; found: 426.1478.

5.1.6.15. N-((4-(1H-Pyrazol-4-yl)phenyl)(4-chlorophenyl)methyl) propan-2-amine ***22a***. Yellow solid (yield, 27%), mp: 78–80 °C. ^{1}H NMR (500 MHz, $CDCl_3$) δ 7.84–7.79 (m, 2H), 7.44 (d, J = 8.1 Hz, 2H), 7.35 (dd, J = 8.4, 3.1 Hz, 4H), 7.24 (d, J = 8.4 Hz, 2H), 4.95 (s, 1H), 2.75 (dt, J = 12.7, 6.3 Hz, 1H), 1.09 (dd, J = 6.2, 3.6 Hz, 6H). ^{13}C NMR (100 MHz, $CDCl_3$) δ 141.5, 140.9, 132.9, 131.5, 130.9, 128.8, 128.7, 128.0, 126.0, 122.3, 63.4, 46.7, 22.6. ESI-MS (*m/z*): 326 [M + 1]$^+$. HRMS (ESI): *m/z* calcd for ($C_{19}H_{20}ClN_3$ + H)$^+$: 326.1424; found: 326.1456.

5.1.6.16. N-((4-(1H-Pyrazol-4-yl)phenyl)(4-chlorophenyl)methyl)-2-methylpropan-1-amine ***22b***. Yellow solid (yield, 40%), mp: 71–73 °C. ^{1}H NMR (500 MHz, $CDCl_3$) δ 7.82 (s, 2H), 7.44 (d, J = 8.2 Hz, 2H), 7.37 (dd, J = 8.2, 5.7 Hz, 4H), 7.24 (d, J = 8.4 Hz, 2H), 4.77 (s, 1H), 2.44–2.32 (m, 2H), 1.76 (dt, J = 13.3, 6.7 Hz, 1H), 0.92 (dd, J = 6.6, 1.3 Hz, 6H). ^{13}C NMR (100 MHz, $CDCl_3$) δ 142.1, 141.6, 132.80, 131.5, 130.9, 129.5, 128.7, 128.7, 127.8, 126.0, 122.4, 66.6, 54.7, 28.3, 20.7. ESI-MS (*m/z*): 340 [M + 1]$^+$. HRMS (ESI): *m/z* calcd for ($C_{20}H_{22}ClN_3$ + H)$^+$: 340.1581; found: 340.1580.

5.1.6.17. N-((4-(1H-Pyrazol-4-yl)phenyl)(4-chlorophenyl)methyl)-2-methylpropan-2-amine ***22c***. White solid (yield, 33%), mp: 85–87 °C. ^{1}H NMR (500 MHz, $CDCl_3$) δ 7.82 (s, 2H), 7.42 (d, J = 8.2 Hz, 2H), 7.39 (d, J = 8.4 Hz, 2H), 7.35 (d, J = 8.2 Hz, 2H), 7.24 (d, J = 8.4 Hz, 2H), 5.00 (s, 1H), 1.08 (s, 9H). ^{13}C NMR (100 MHz, DMSO-d_6) δ 138.7, 137.1, 133.3, 132.6, 131.3, 130.2, 129.3, 128.8, 126.1, 121.3, 60.9, 59.9, 27.0. ESI-MS (*m/z*): 340 [M + 1]$^+$. HRMS (ESI): *m/z* calcd for ($C_{20}H_{22}ClN_3$ + H)$^+$: 340.1581; found: 340.1570.

5.1.6.18. N-((4-(1H-Pyrazol-4-yl)phenyl)(4-chlorophenyl)methyl) cyclopropanamine ***22d***. White solid (yield, 21%), mp: 62–64 °C. ^{1}H NMR (500 MHz, $CDCl_3$) δ 7.83 (s, 2H), 7.45 (d, J = 8.0 Hz, 2H), 7.35–7.25 (m, 6H), 4.90 (s, 1H), 2.12–2.05 (m, 1H), 0.45–0.35 (m, 4H). ESI-MS (*m/z*): 324 [M + 1]$^+$. HRMS (ESI): *m/z* calcd for ($C_{19}H_{18}ClN_3$ + H)$^+$: 324.1268; found: 324.1266.

5.1.6.19. N-((4-(1H-Pyrazol-4-yl)phenyl)(4-chlorophenyl)methyl) cyclohexanamine ***22e***. White solid (yield, 54%), mp: 69–71 °C. ^{1}H NMR (500 MHz, $CDCl_3$) δ 7.81 (s, 2H), 7.43 (d, J = 8.2 Hz, 2H), 7.35 (dd, J = 8.5, 2.5 Hz, 4H), 7.29–7.24 (m, 2H), 5.01 (s, 1H), 2.44–2.32 (m, 1H), 1.95 (d, J = 6.6 Hz, 2H), 1.69 (dd, J = 9.2, 3.4 Hz, 2H), 1.21–1.03 (m, 6H). ESI-MS (*m/z*): 366 [M + 1]$^+$. HRMS (ESI): *m/z* calcd for ($C_{22}H_{24}ClN_3$ + H)$^+$: 366.1737; found: 366.1696.

5.1.6.20. N-((4-(1H-Pyrazol-4-yl)phenyl)(4-chlorophenyl)methyl)aniline ***22f***. Yellow solid (yield, 25%), mp: 69–71 °C. ^{1}H NMR (500 MHz, $CDCl_3$) δ 7.85 (s, 2H), 7.47 (d, J = 8.2 Hz, 2H), 7.35–7.29 (m, 6H), 7.13 (t, J = 7.9 Hz, 2H), 6.72 (t, J = 7.3 Hz, 1H), 6.55 (d, J = 8.2 Hz, 2H), 5.47 (s, 1H). ESI-MS (*m/z*): 360 [M + 1]$^+$. HRMS (ESI): *m/z* calcd for ($C_{22}H_{18}ClN_3$ + H)$^+$: 359.1189; found: 359.1200.

5.1.6.21. 1-(4-(1H-Pyrazol-4-yl)phenyl)-N-benzyl-1-(4-chlorophenyl) methanamine ***22g***. Yellow solid, yield 39%, mp: 63–69 °C. ^{1}H NMR (500 MHz, $CDCl_3$) δ 7.83 (s, 2H), 7.46 (d, J = 7.6 Hz, 2H), 7.44–7.38 (m, 4H), 7.38–7.26 (m, 7H), 4.85 (s, 1H), 3.76 (s, 2H). ^{13}C NMR (100 MHz, $CDCl_3$) δ 142.3, 141.8, 140.0, 132.8, 131.4, 128.9, 128.7, 128.6, 128.5, 128.2, 127.8, 127.1, 126.1, 122.5, 65.4, 51.1. ESI-MS (*m/z*): 374 [M + 1]$^+$. HRMS (ESI): *m/z* calcd for ($C_{23}H_{20}ClN_3$ + H)$^+$: 374.1424; found: 374.1454.

5.1.6.22. 2-(((4-(1H-Pyrazol-4-yl)phenyl)(4-chlorophenyl)methyl) amino)ethanol ***22h***. Yellow syrup (yield, 35%), ^{1}H NMR (500 MHz, $CDCl_3$) δ 7.78 (s, 2H), 7.43 (d, J = 7.6 Hz, 2H), 7.37–7.30 (s, 4H), 7.27 (s, 1H), 4.85 (s, 1H), 3.73 (s, 2H), 2.79 (s, 2H). ESI-MS (*m/z*): 328 [M + 1]$^+$. HRMS (ESI): *m/z* calcd for ($C_{18}H_{18}ClN_3O$ + H)$^+$: 328.1217; found: 328.1212.

5.1.6.23. N^1-((4-(1H-Pyrazol-4-yl)phenyl)(4-chlorophenyl)methyl) ethane-1,2-diamine ***22i***. Yellow syrup (yield, 42%), ^{1}H NMR (500 MHz, $CDCl_3$) δ 7.78 (s, 2H), 7.43 (d, J = 8.0 Hz, 2H), 7.35 (t, J = 8.0 Hz, 4H), 7.28 (d, J = 8.0 Hz, 2H), 4.81 (s, 1H), 3.72 (q, J = 7.0 Hz, 1H), 2.86 (t, J = 5.6 Hz, 2H), 2.67 (t, J = 5.6 Hz, 2H), 1.26 (t, J = 7.0 Hz, 2H). ESI-MS (*m/z*): 327 [M + 1]$^+$. HRMS (ESI): *m/z* calcd for ($C_{18}H_{19}ClN_4$ + H)$^+$: 327.1376; found: 327.1380.

5.2. Pharmacological assay

5.2.1. Akt1 assay

AKT1/PKBα Kinase Assay Kit (catalog No. 32-021) and active recombinant AKT1 kinase were commercially available from UP-STATE (acquired by Merck Millipore, Billerica, MA). 4 ng of Akt1 in 8 μL of 2.5× kinase buffer [62.5 mM Tris–HCl (pH 7.5), 25 mM $MgCl_2$, 12.5 mM β-glycerophosphate, 0.25 mM Na_3VO_4, 5 mM dithiothreitol (DTT)], was mixed with 2 μL of dimethyl sulfoxide (DMSO) vehicle or each of the compound (indicated concentrations), incubated at room temperature for 5 min and 10 μL of ATP/substrate cocktail (20 mM ATP, 3 mM eNOS served as substrate) was added. After incubation at room temperature for 30 min, add 20 μL of 50 mM ethylenediaminetetraacetic acid (EDTA) (pH 8.0) and terminate the reaction. Then, PKB/Akt1 kinase activity was analyzed according to the manufacturer's instructions.

5.2.2. Anti-proliferative activity assay

The cytotoxic activity of the tested compounds in OVCAR-8 (Ovarian Adenocarcinoma), HL-60 (Promyelocytic Leukemia) and HCT116 (Human Colon Cancer) cells was measured using the MTT (3-(4,5-dimethylthiazol-2-yl)-2,5-diphenyltetrazolium bromide, a tetrazole) method. Cells were seeded in 96-well microtiter plates (at a density of 4000 cells per well) for overnight attachment and exposed to each of the compound (1.0–100.0 μM) for 72 h. The MTT solution (5.0 mg/mL in RPIM 1640 medium; Sigma–Aldrich) was added (20.0 μl/well), and plates were incubated for a further 4 h at 37 °C. The purple formazan crystals were dissolved in 100.0 μL of DMSO. After 5 min, the plates were read on an automated microplate spectrophotometer (Bio-Tek Instruments, Winooski, VT) at 570 nm. Assays were performed in triplicate on three independent experiments. The concentration of drug inhibiting 50% of cells (IC_{50}) was calculated using the software of dose-effect analysis with microcomputers.

5.2.3. Apoptosis assay

To analysis apoptosis, OVCAR-8 cells (5×10^4 cells/ml, 5 ml) were cultured in 25 cm^2 flasks and treated with vehicle to test compounds (20 μM). After 48 h of treatments, cells were harvested and quickly washed twice with ice-cold PBS. Detection of apoptosis by FACSCalibur flow cytometer (Becton Dickinson, Lincoln Park, NJ) was performed using the Annexin V-FITC/Propidium iodide (PI) apoptosis detection kit (BioVision, Mountain View, CA).

5.2.4. Western blotting assay

OVCAR-8 cells were harvested, washed with ice-cold 1× phosphate-buffered saline (PBS), and lysed in immunoprecipitation assay buffer [150 mM NaCl, 50 mM Tris, 2 mM ethyleneglycol-bis(b-aminoethylether), 2 mM EDTA, 25 mM NaF, 25 mM b-glycerophosphate, 0.2% TritonX-100, 0.3% Nonidet P-40, and 0.1 mM phenylmethylsulfonyl fluoride]. Cellular debris was pelleted by centrifugation at 13,000 rpm for 30 min at 4 °C. The concentrations of the total lysate protein were measured using a standard Bradford assay (Bio-Rad, San Diego, CA). For Western blot analysis, 40–80 μg of protein from the total cell lysate was electrophoresed by SDS-PAGE. The proteins were then transferred to nitrocellulose membrane (Pierce Chemical) and probed with primary antibodies followed by horseradish peroxidase-labeled secondary antibodies. Proteins were visualized using enhanced chemiluminescence (Pierce Chemical).

Acknowledgment

We thank Mrs. Jianyang Pan (Pharmaceutical Informatics Institute, Zhejiang University) for performing the NMR spectrometry. This study was financially supported by National Natural Science Foundation of China (No. 81001359), China Postdoctoral Science Foundation (No. 201003734), Zhejiang province Provincial Natural Science Foundation of China (LY13H300002), and Program for Zhejiang Leading Team of S&T Innovation.

Appendix A. Supplementary data

Supplementary data related to this article can be found at http://dx.doi.org/10.1016/j.ejmech.2013.11.036.

References

[1] S.P. Staal, Molecular cloning of the Akt oncogene and its human homologues AKT1 and AKT2: amplification of AKT1 in a primary human gastric adenocarcinoma, Proc. Natl. Acad. Sci. U. S. A. 84 (1987) 5034–5037.
[2] J.Q. Cheng, B. Ruggeri, W.M. Klein, G. Sonoda, D.A. Altomare, D.K. Watson, J.R. Testa, Amplification of AKT2 in human pancreatic cancer cells and inhibition of AKT2 expression and tumorigenicity by antisense RNA, Proc. Natl. Acad. Sci. U.S.A. 93 (1996) 3636–3641.
[3] R.T. Joseph, B. Alfonso, AKT plays a central role in tumorigenesis, Proc. Natl. Acad. Sci. U.S.A. 98 (2001) 10983–10985.
[4] L.C. Cantley, The phosphoinositide 3-kinase pathway, Science 296 (2002) 1655–1657.
[5] K.M. Nicholson, N.G. Anderson, The protein kinase B/Akt signalling pathway in human malignancy, Cell. Signal. 14 (2002) 381–395.
[6] J.Q. Cheng, C.W. Lindsley, G.Z. Cheng, H. Yang, S.V. Nicosia, The Akt/PKB pathway: molecular target for cancer drug discovery, Oncogene 24 (2005) 7482–7492.
[7] T.F. Franke, PI3K/Akt: getting it right matters, Oncogene 27 (2008) 6473–6488.
[8] L. Salmena, A. Carracedo, P.P. Pandolfi, Tenets of PTEN tumor suppression, Cell 133 (2008) 403–414.
[9] S.R. Datta, A. Brunet, M.E. Greenberg, Cellular survival: a play in three Akts, Genes Dev. 13 (1999) 2905–2927.
[10] M.P. Scheid, J.R. Woodgett, PKB/AKT: functional insights from genetic models, Nat. Rev. Mol. Cell Biol. 2 (2001) 760–768.
[11] E. Tokunaga, A. Kataoka, Y. Kimura, E. Oki, K. Mashino, K. Nishida, T. Koya, M. Morita, Y. Kakeji, H. Baba, S. Ohno, Y. Maehara, The association between Akt activation and resistance to hormone therapy in metastatic breast cancer, Eur. J. Cancer 42 (2006) 629–635.
[12] E. Oki, H. Baba, E. Tokunaga, T. Nakamura, N. Ueda, M. Futatsugi, K. Mashino, M. Yamamoto, M. Ikebe, Y. Kakeji, Y. Maehara, AKT phosphorylation associates with LOH of PTEN and leads to chemoresistance for gastric cancer, Int. J. Cancer 117 (2005) 376–380.
[13] M.E. Mattmann, S.L. Stoops, C.W. Lindsley, Inhibition of Akt with small molecules and biologics: historical perspective and current status of the patent landscape, Expert. Opin. Ther. Pat. 21 (2011) 1309–1338.
[14] C.W. Lindsley, S.F. Barnett, M.E. Layton, M.T. Bilodeau, The PI3K/Akt pathway: recent progress in the development of ATP-competitive and allosteric Akt kinase inhibitors, Curr. Cancer Drug Targets 8 (2008) 7–18.
[15] E.J. Meuillet, Novel inhibitors of AKT: assessment of a different approach targeting the Pleckstrin homology domain, Curr. Med. Chem. (2011).
[16] W. Marsh Rde, C.M. Rocha Lima, D.E. Levy, E.P. Mitchell, K.M. Rowland Jr., A.B. Benson 3rd, A phase II trial of perifosine in locally advanced, unresectable, or metastatic pancreatic adenocarcinoma, Am. J. Clin. Oncol. 30 (2007) 26–31.
[17] N.B. Leighl, S. Dent, M. Clemons, T.A. Vandenberg, R. Tozer, D.G. Warr, R.M. Crump, D. Hedley, G.R. Pond, J.E. Dancey, M.J. Moore, A phase 2 study of perifosine in advanced or metastatic breast cancer, Breast Cancer Res. Treat. 108 (2008) 87–92.
[18] T.A. Yap, L. Yan, A. Patnaik, I. Fearen, D. Olmos, K. Papadopoulos, R.D. Baird, L. Delgado, A. Taylor, L. Lupinacci, R. Riisnaes, L.L. Pope, S.P. Heaton, G. Thomas, M.D. Garrett, D.M. Sullivan, J.S. de Bono, A.W. Tolcher, First-in-man clinical trial of the oral pan-AKT inhibitor MK-2206 in patients with advanced solid tumors, J. Clin. Oncol. 29 (2011) 4688–4695.
[19] B.R. Davies, H. Greenwood, P. Dudley, C. Crafter, D.H. Yu, J. Zhang, J. Li, B. Gao, Q. Ji, J. Maynard, S.A. Ricketts, D. Cross, S. Cosulich, C.C. Chresta, K. Page, J. Yates, C. Lane, R. Watson, R. Luke, D. Ogilvie, M. Pass, Preclinical pharmacology of AZD5363, an inhibitor of AKT: pharmacodynamics, antitumor activity, and correlation of monotherapy activity with genetic background, Mol. Cancer Ther. 11 (2012) 873–887.
[20] T.A. Yap, M.I. Walton, K.M. Grimshaw, R.H. Te Poele, P.D. Eve, M.R. Valenti, A.K. de Haven Brandon, V. Martins, A. Zetterlund, S.P. Heaton, K. Heinzmann, P.S. Jones, R.E. Feltell, M. Reule, S.J. Woodhead, T.G. Davies, J.F. Lyons, F.I. Raynaud, S.A. Eccles, P. Workman, N.T. Thompson, M.D. Garrett, AT13148 is a novel, oral multi-AGC kinase inhibitor with potent pharmacodynamic and antitumor activity, Clin. Cancer Res. 18 (2012) 3912–3923.
[21] X. Dong, X. Zhou, H. Jing, J. Chen, T. Liu, B. Yang, Q. He, Y. Hu, Pharmacophore identification, virtual screening and biological evaluation of prenylated flavonoids derivatives as PKB/Akt1 inhibitors, Eur. J. Med. Chem. 46 (2011) 5949–5958.

[22] A. Donald, T. McHardy, M.G. Rowlands, L.J. Hunter, T.G. Davies, V. Berdini, R.G. Boyle, G.W. Aherne, M.D. Garrett, I. Collins, Rapid evolution of 6-phenylpurine inhibitors of protein kinase B through structure-based design, J. Med. Chem. 50 (2007) 2289–2292.
[23] K.D. Freeman-Cook, C. Autry, G. Borzillo, D. Gordon, E. Barbacci-Tobin, V. Bernardo, D. Briere, T. Clark, M. Corbett, J. Jakubczak, S. Kakar, E. Knauth, B. Lippa, M.J. Luzzio, M. Mansour, G. Martinelli, M. Marx, K. Nelson, J. Pandit, F. Rajamohan, S. Robinson, C. Subramanyam, L. Wei, M. Wythes, J. Morris, Design of selective, ATP-competitive inhibitors of Akt, J. Med. Chem. 53 (2010) 4615–4622.
[24] M. Addie, P. Ballard, D. Buttar, C. Crafter, G. Currie, B.R. Davies, J. Debreczeni, H. Dry, P. Dudley, R. Greenwood, P.D. Johnson, J.G. Kettle, C. Lane, G. Lamont, A. Leach, R.W. Luke, J. Morris, D. Ogilvie, K. Page, M. Pass, S. Pearson, L. Ruston, Discovery of 4-amino-*N*-[(1*S*)-1-(4-chlorophenyl)-3-hydroxypropyl]-1-(7*H*-pyrrolo[2,3-*d*]pyrimidin-4-yl)piperidine-4-carboxamide (AZD5363), an orally bioavailable, potent inhibitor of Akt kinases, J. Med. Chem. 56 (2013) 2059–2073.
[25] C.M. Venkatachalam, X. Jiang, T. Oldfield, M. Waldman, LigandFit: a novel method for the shape-directed rapid docking of ligands to protein active sites, J. Mol. Graph. Model. 21 (2003) 289–307.
[26] R. Dayam, T. Sanchez, O. Clement, R. Shoemaker, S. Sei, N. Neamati, Beta-diketo acid pharmacophore hypothesis. 1. Discovery of a novel class of HIV-1 integrase inhibitors, J. Med. Chem. 48 (2005) 111–120.
[27] W.J. Li, D.P. Nelson, M.S. Jensen, R.S. Hoerrner, D.W. Cai, R.D. Larsen, P.J. Reider, An improved protocol for the preparation of 3-pyridyl- and some arylboronic acids, J. Org. Chem. 67 (2002) 5394–5397.
[28] S. Lucas, R. Heim, C. Ries, K.E. Schewe, B. Birk, R.W. Hartmann, In vivo active aldosterone synthase inhibitors with improved selectivity: lead optimization providing a series of pyridine substituted 3,4-dihydro-1*H*-quinolin-2-one derivatives, J. Med. Chem. 51 (2008) 8077–8087.
[29] C.C. Kumar, V. Madison, Akt crystal structure and Akt-specific inhibitors, Oncogene 24 (2005) 7493–7501.
[30] M.W. Karaman, S. Herrgard, D.K. Treiber, P. Gallant, C.E. Atteridge, B.T. Campbell, K.W. Chan, P. Ciceri, M.I. Davis, P.T. Edeen, R. Faraoni, M. Floyd, J.P. Hunt, D.J. Lockhart, Z.V. Milanov, M.J. Morrison, G. Pallares, H.K. Patel, S. Pritchard, L.M. Wodicka, P.P. Zarrinkar, A quantitative analysis of kinase inhibitor selectivity, Nat. Biotechnol. 26 (2008) 127–132.
[31] A. Krammer, P.D. Kirchhoff, X. Jiang, C.M. Venkatachalam, M. Waldman, LigScore: a novel scoring function for predicting binding affinities, J. Mol. Graph. Model. 23 (2005) 395–407.
[32] D.K. Gehlhaar, G.M. Verkhivker, P.A. Rejto, C.J. Sherman, D.B. Fogel, L.J. Fogel, S.T. Freer, Molecular recognition of the inhibitor AG-1343 by HIV-1 protease: conformationally flexible docking by evolutionary programming, Chem. Biol. 2 (1995) 317–324.
[33] I. Muegge, Y.C. Martin, A general and fast scoring function for protein-ligand interactions: a simplified potential approach, J. Med. Chem. 42 (1999) 791–804.